PAPER

Interaction of high-intensity focused ultrasound with polymers at the atomistic scale

IOP Publishing Nanotechnology
Nanotechnology 32 (2021) 045707 (9pp) https://doi.org/10.1088/1361-6528/abbfd2

Interaction of high-intensity focused ultrasound with polymers at the atomistic scale

Kaiyuan Peng, Shima Shahab and Reza Mirzaeifar

Department of Mechanical Engineering, Virginia Tech, Blacksburg, Virginia 24061, United States of America

E-mail: rmirzaei@vt.edu

Received 26 June 2020, revised 3 September 2020
Accepted for publication 9 October 2020
Published 28 October 2020

Abstract

Experiments show that high-intensity focused ultrasound (HIFU) is a promising stimulus with multiple superior and unique capabilities to induce localized heating and achieve temporal and spatial thermal effects in the polymers, noninvasively. When polymers are subjected to HIFU, they heat up differently compared to the case they are subjected to heat sources directly; however, the origins of this difference are still entirely unknown. We hypothesize that the difference in the macroscale response of polymers subjected to HIFU strongly depends on the polymer chains, composition, and structure, i.e. being crystalline or amorphous. In this work, this hypothesis is investigated by molecular dynamics studies at the atomistic level and verified by experiments at the macroscopic scale. The results show that the viscoelasticity, measured by stress–strain phase lag, the reptation motion of the chains, and the vibration-induced local mobility quantified by the root mean square fluctuation contribute to the observed difference in the HIFU-induced thermal effects. This unravels the unknown mechanisms behind stimulating the polymers by HIFU, and paves the way in front of using this method in future applications.

Keywords: high-intensity focused ultrasound (HIFU), stimuli-responsive polymers, molecular dynamics (MD)

(Some figures may appear in colour only in the online journal)

1. Introduction

Stimuli-responsive polymers, i.e. shape memory and shape-changing polymers, have been intensively investigated for their applications in controlled drug delivery [1–4], sensing and biosensing [5, 6], smart coating [7], soft robotics [8, 9] and flexible electronics [10, 11]. The choice of an environmental trigger for stimulating polymers is one of the critical factors. Although direct heat is one of the most commonly used triggers, it is not always practical and safe, especially for heat-sensitive applications [12–14]. Consequently, other forms of noninvasive actuating mechanisms such as irradiation (UV, IR, and solar), magnetic field, electric current, among others, have come to the forefront [15–23]. However, most of these triggers significantly lower the efficiency of the responsiveness of the polymers. As an alternative to the conventional stimulus type, it has been shown that the polymeric materials are ultrasound-stimulus-responsive, with controlled multifunction [3, 24]. High-intensity focused ultrasound (HIFU) is an entirely different and promising stimulus due to its superior and unique capability. HIFU could induce localized heating and achieve temporal and spatial effects in polymers, by adjusting the geometric and chemical properties of the polymer, ultrasound frequency, exposure time, intensity as well as the position of ultrasound focusing, all while being noninvasive.

HIFU transmits and focuses acoustic energy from a transducer into a small focal volume. The sound waves are directed to interact with polymer chains in a selected area, heating the polymers locally, and causing a significant thermal effect on the focal point, while the surrounding area is not significantly affected. When the mechanical waves pass

through the polymer matrix, damping losses will occur due to viscous shearing and relaxation. Ultrasonic waves, as a kind of mechanical wave, can make a polymer behave in a pattern of forced vibration, and thus exert alternative stress at every chain of the polymer matrix. For viscoelastic polymeric materials, change of strain lags behind that of stress, which induces the internal friction and the energy absorption during HIFU absorption. The energy absorption pattern has two types, one part of the energy is dissipated and transformed into heat, and the remaining part is stored by elastic deformation of polymer chains. The ultrasonic energy converts to heat through internal friction, which induces the temperature rise of the polymer. This localized heating eliminates the need to incorporate individual or responsive particles employed for use as noninvasive triggers [25]; therefore, ultrasound can be considered one of the most potent modalities for spatio-temporal stimulation of polymers in an on-off switch manner.

Unlike conventional heating, it has been observed that different polymers possess different HIFU-induced thermal effects [26]. However, the research related to the fundamental mechanisms behind this phenomenon, particularly at the atomistic scale, is still limited. Liu *et al* reported heating rates and equilibrium temperatures about HIFU heated polyethylene (PE), poly(methyl methacrylate) (PMMA), polycarbonate (PC), polystyrene (PS), Nylon-6 (PA-6) and polypropylene (PP) [27]. They hypothesized that the variation in thermal effects for various polymers could be attributed to the different internal frictions between their macromolecular chains. Bruinewoud also investigated the ultrasound-induced thermal effects of a set of polymers, including PMMA, polyurethane (PUR) and poly (ethylene-vinyl acetate) (PEVA) [28]. Coralie and co-workers reported the correlation between the particle velocity distribution and PMMA heating rate by HIFU [29], and they concluded the particle velocity distribution and the sample thickness determine the heating response of the polymer. Although these experimental results indicate that the ultrasound-induced thermal effects in polymers are affected by many factors, to understand the mechanisms completely only by experiments is extremely challenging. This is because tracking the interaction between the polymer and ultrasonic waves at the atomistic scale by the experiments is very difficult. As an alternative, here, we utilize computational models to explore how the HIFU triggers thermal actuation of polymers, and how the atomistic structure of the polymer interacts with the representative mechanism. Molecular dynamics (MD) simulations have been used as a unique tool for studying the mechanical and thermal properties of polymeric materials [30–36]. The trajectory history of every atom in the polymeric system during the ultrasonic actuation, as well as the evolution of the chain orientation can be recorded.

In this study, we investigate the ultrasound-induced thermal effect at the atomistic scale by MD simulation (using the LAMMPS package [37]). Related experiments were performed to support the findings of the computational model. We particularly focus on exploring the role of chain arrangement and structure on the thermal effects. Low-density polyethylene (LDPE) and high-density polyethylene (HDPE) are studied as a counterpart. To our best knowledge, this is the first study on the ultrasound-induced thermal effects of polymeric materials at the atomistic scale, which can explain the observed thermal responses at the macroscale.

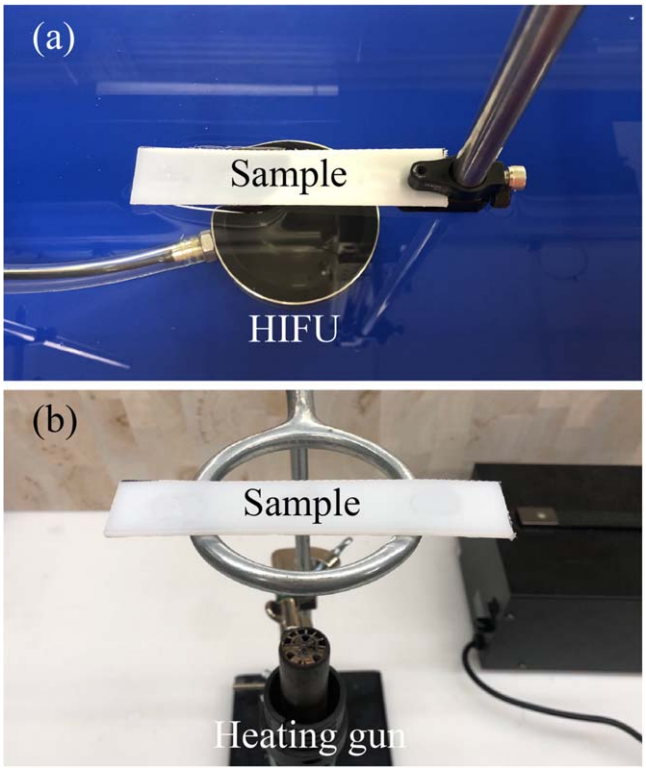

Figure 1. (a) Experimental setup of the polymer filament with a fixed-free boundary condition exposed to harmonic acoustic pressure at 0.5 MHz; the geometric center of the filament is located in the focal area. (b) Heating gun setup.

Table 1. Geometric details of the modified H-104–4 A SONIC Concepts HIFU transducer.

Outer diameter	Intensity focus watts	Focal width (dia.)	Focal length
64 mm	3267.56 W cm^{-2}	3.02 mm	50 mm

2. Methods

2.1. Experimental scenarios

Before delivering the results from MD simulations, two experimental scenarios about actuating the polymers with HIFU and direct heat are shown here. Firstly, in figure 1(a), a PE filament with a dimension of 125 × 25 × 2.38 mm was suspended at the surface of deionized water. Next, the filament was exposed to a harmonic acoustic pressure field at 0.5 MHz generated by a modified H-104–4 A SONIC Concepts HIFU transducer. The transducer, actuated with 30 V voltage at 6 W input power, was turned on in continuous mode for 30 s. The geometric details of the modified HIFU transducer are listed in table 1. The distance between the

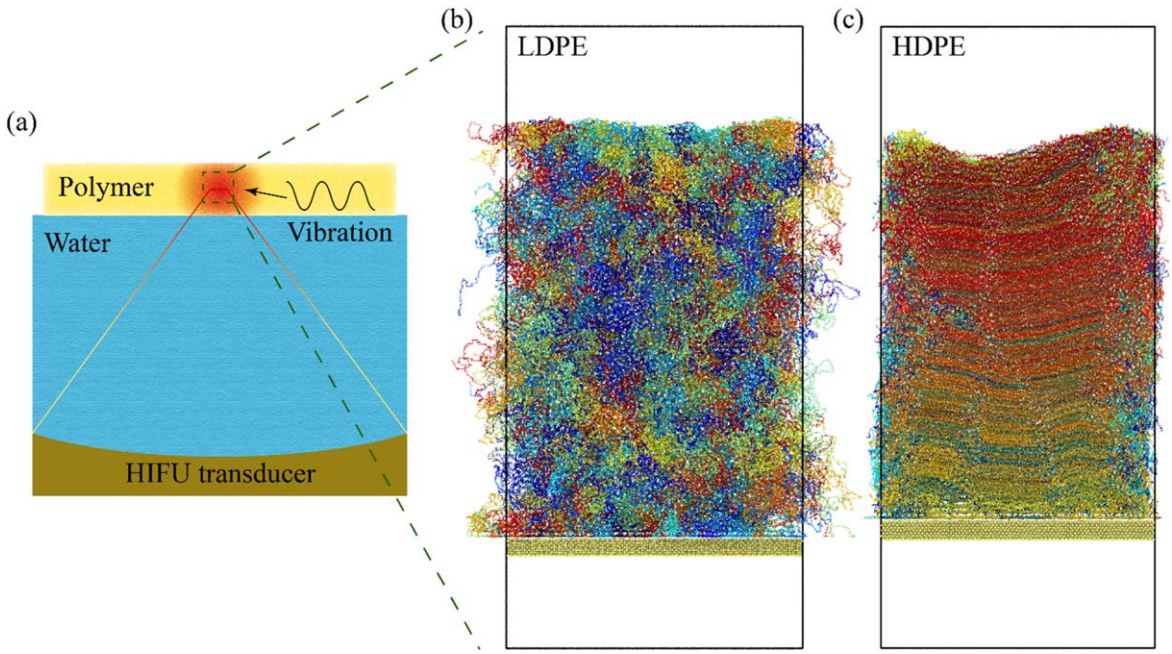

Figure 2. Schematics of (a) typical ultrasound-induced heating setup, and MD simulation setup for (b) LDPE and (c) HDPE system.

transducer and the filament is 50 mm, which was adjusted by a positioning system, to make the geometric center of the filament located at the focal area of the transducer. The water level in the tank was maintained, such that the bottom part of the filament was submerged in water and the focal point of the HIFU transducer located at the central portion of the filament. The power of the transducer was maintained below a threshold level (10 W) to prevent degradation of the sample [3].

A FLIR C2 thermal imaging camera was fixed to capture thermal images focusing on the exposure area of the HIFU. The camera has an imaging rate of around 0.25 Hz. The duration of ultrasonic actuation is 30 continuous seconds, with most thermal measurements reaching 40 s to make sure the entire thermal history is captured. Data is processed with FLIR Tools software. For the direct heat method, the sample was suspended 80 mm above a heating gun in figure 1(b). The exhaust temperature of the hot air was set at 180 °C, to make the temperature rises by hot air and ultrasound comparable.

2.2. Simulation methods

In the following sections, we regard amorphous polyethylene as LDPE and crystalline polyethylene as HDPE, shown in figure 2. In the MD simulation, the polymeric systems were built by a self-avoiding random-walk algorithm initially, then equilibrated under different conditions to create an amorphous structure (LDPE) and a crystalline structure (HDPE) separately. The details of the equilibration conditions are discussed as follows.

To avoid the influence of molecular weights (chain lengths), both systems contain 576 chains with chain length $N = 400$, in a total of 230 400 atoms. For LDPE, the initial geometry is first melted by increasing the temperature from 300 to 500 K. The system is further annealed back to 300 K, followed by an equilibration through NPT ensemble until the density reaches the targeted value ($\sim$0.9 g cm^{-3}). To form the HDPE structure, the system is melted at 500 K, then pre-stretched along the z-direction. After that, the oriented melt is suddenly quenched down to 330 K, then an NPT ensemble runs for 60 ns at 330 K to guarantee the crystallization grows sufficiently. Finally, the system is cooled down to 300 K and equilibrated again.

The simulation domains (shown in figure 2), which are periodic in x and y directions, contain HDPE and LDPE on the substrate. Polymeric chains are rendered in different colors to show the structure variation. We use the potential force field that is introduced in [38, 39] for polyethylene-like materials. A cutoff distance of 10.0 Å for the Lennard-Jones interactions and 1 fs for time step are applied for all simulations.

As mentioned early, the temperature rises for HDPE and LDPE are similar manner by direct heat. Therefore, it is interesting to use MD simulations to explore the reasons why the heating rate varies when they are subjected to HIFU. In the simulation, the substrate is vertically oscillated at multiple frequencies to imitate the mechanical vibration caused by ultrasonic waves. The substrate is maintained at 300 K to physically represent the heat sink at room temperature, while no temperature restriction is placed on the polymer system (NVE ensemble). The velocity of the substrate in the z-direction is $v_0 = A\omega \cos(\omega t)$, where A is the amplitude and ω is the frequency. A summary of all parameters applied in the MD simulations is listed in table 2. With regard to HIFU specification, the amplitude and frequency here are proportional to the ultrasound input power and frequency.

Table 2. Parameters applied in the MD simulations.

	Frequency (GHz)	Amplitude (nm)	Duration (ns)
Case 1	8.33	0.5	1
Case 2	11.1	0.5	1
Case 3	12.5	0.5	1
Case 4	8.33	2	20

3. Results and discussion

3.1. Experimental results

The samples were exposed to the ultrasonic waves or hot air for ~30 s. The profile of the highest temperatures at the focal point on HDPE and LDPE samples is shown in figure 3(a). For all cases, the initial temperatures are around room temperature (25 °C–27 °C). Heated by hot air, the temperatures for HDPE and LDPE are ramped almost linearly, with $R^2 = 0.9988$ and 0.9997 separately. However, when the samples are stimulated by HIFU, the temperature rises are nonlinear and saturated after ~15 s. In the initial 5 s, the rate of temperature increase for LDPE and HDPE are 2.2 °C · s^{-1} and 0.88 °C · s^{-1} separately, so the observed temperature rate for LDPE is larger than HDPE by an amount of 150%. The equilibrium temperature for LDPE, after 30 s exposure to HIFU, is ~48 °C, which is ~10 °C higher than that of HDPE. Figures 3(b) and (c) show the induced thermal field of the HDPE and LDPE filaments when $t = 25$ s. In the image, the spot in the center has the maximum temperature. This indicates the thermal effect of focused ultrasound on PE materials is highly concentrated and localized.

3.2. MD simulation

We systematically study the thermal effect of HIFU on HDPE and LDPE across a wide range of oscillation times, amplitudes (A) and frequencies (f). The temperature evolution with a time duration of 1 ns for $A = 0.5$ nm, as well as $f = 8.33$, 11.1 and 12.5 GHz are shown in figures 4(a)–(c). In figure 4(d), the substrate is oscillating for 20 ns at $A = 2$ nm and $f = 8.33$ GHz. Upon figures 4(a)–(c), we found the frequency increase raises the polymer temperature in general. In addition, in comparison of figures 4(b) and (c), the heating rate for LDPE is higher than that of HDPE, which is consistent with the experimental results. It is also interesting to note that although the temperature rise in figure 4(a) is almost negligible due to the relatively low frequency, the accumulated thermal effect becomes considerable when the amplitude and time scale enlarge at the same frequency, which results in a prominent temperature rise as shown in figure 4(d). The applicable HIFU frequency (~MHz) is orders of magnitude smaller than that in the MD simulation (~GHz), but we believe that the MD simulation here is able to replicate the heating mechanism in a manner which is consistent with the actual experiment. Firstly, although acoustic energy with higher frequencies is lost more along the beam path before reaching the target, the mechanism of the vibration-induced heating is not dependent on that. The frequency-dependent energy absorption efficiency of the sample is beyond the scope of this work. Secondly, because of the limit of computational resources, the time scale of most MD simulation is at the range of several nanoseconds (10^{-9} s). This is a very common problem in almost all MD simulations, but researchers show MD simulations are able to capture the critical mechanism for ultrasonic actuation problems [32]. Therefore, we believe our MD results can shed light on the mechanism at the macroscale.

3.2.1. Viscoelasticity for entire polymeric system. Now the open question is why HDPE and LDPE, with the same chemical composition and chain length, respond differently to the same external excitation. By using MD simulations, we are able to provide a qualitative description of the ultrasonic actuation mechanism in a top-to-bottom manner, in which the microscopic picture of the HIFU-induced vibration is described at different scales from the entire polymer system, single polymeric chain down to single atoms. For the entire polymer system, the heat is generated by the viscoelastic damping, which is highly dependent on the polymer viscoelasticity. Since viscoelasticity is frequency-dependent, the phase lag between stress and stress curves is also related to frequency. The dissipated energy per cycle that transferred into heat can be given as the following energy density function:

$$\delta W = \sigma_0 \epsilon_0 f \int_0^{\frac{2\pi}{f}} \sin \omega t * \cos(ft - \theta) \mathrm{d}t, \tag{1}$$

where σ_0 is the amplitude of stress, ϵ_0 is the amplitude of strain, f is the frequency, θ is the phase lag between the stress and strain curves. Note that the energy into heat δW is in direct proportion to σ_0, ϵ_0, and θ. The frequencies f are 8.33 GHz and 12.5 GHz as shown in figure 5. Figures 5(a) and (c) show the results for HDPE while figures 5(b) and (d) represent LDPE.

The temperature difference between HDPE and LDPE at 8.33 GHz is negligible, and results in subtle phase lags between strain curves and stress curves for both LDEP and HDPE as seen in figure 5. When the frequency increases to 12.5 GHz, LDPE shows an apparent temperature increase. Correspondingly, there is a significant lag between the stress and strain curves in figure 5(d) (shown in the zoom-in plot). Contrary to LDPE, the phase lag change for HDPE between 8.33 and 12.5 GHz becomes slightly larger (figure 5(c)). Besides, the oscillating amplitude of stress/strain curves, at 12.5 GHz is prominently larger than that at 8.33 GHz. Moreover, the stress/strain amplitude for LDPE is larger than that for HDPE at the specific frequencies. Figure 6 shows the relationship between the position of the oscillated substrate and the stress of the polymer at 12.5 GHz, whether the stress change can follow the substrate movement. We can find there is a more pronounced phase delay between the substrate position and the polymer stress curve (labeled as δ) for LDPE in figure 6(b) than that for HDPE in figure 6(a). Hereby, the LDPE is expected to be more difficult to follow the external vibration, such as by ultrasonic actuation, which may cause more viscous internal friction and then generate more heat.

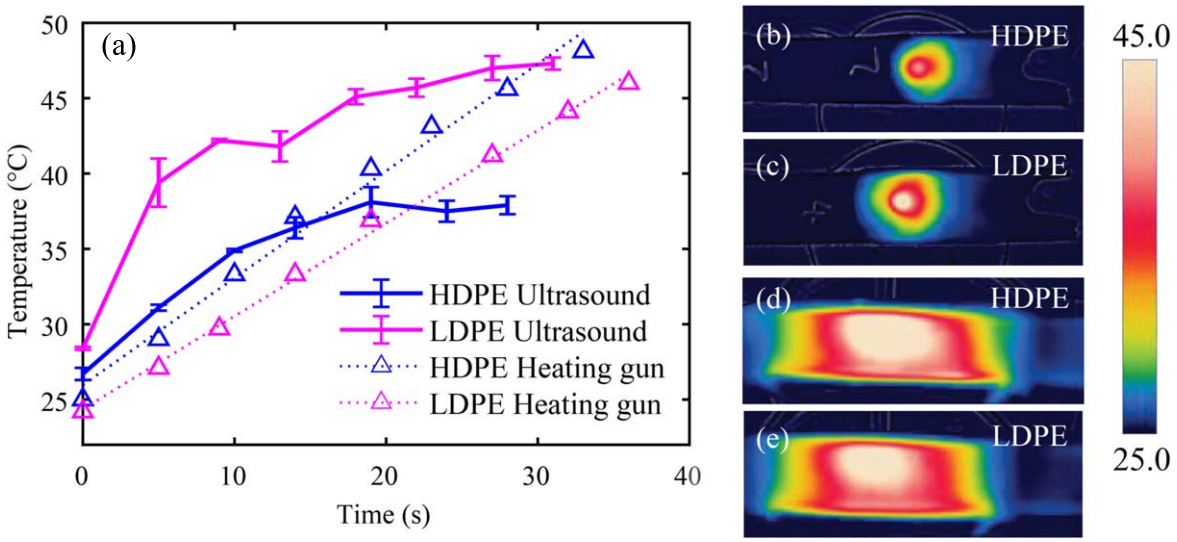

Figure 3. (a) Temperature versus time for HDPE and LDPE induced by HIFU (solid lines) or heating gun (dot lines). Thermal images of (b) HDPE and (c) LDPE filaments under ultrasound, (d) HDPE and (e) LDPE filaments under hot air when $t = \sim 30$ s.

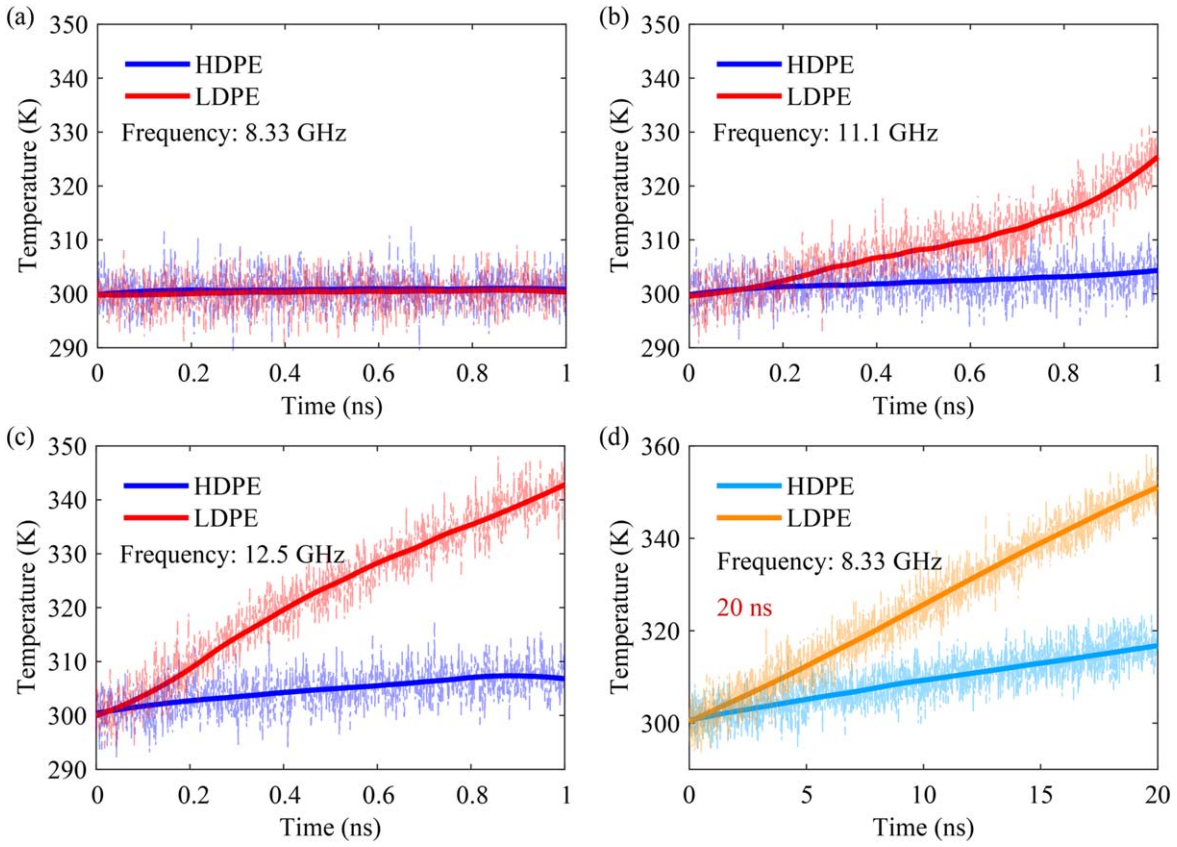

Figure 4. Temperature versus time curve for 1 ns at frequencies of (a) 8.33 GHz, (b) 11.1 GHz, (c) 12.5 GHz, and (d) for 20 ns at a frequency of 8.33 GHz.

3.2.2. Reptation of chains. To investigate the differences in the thermal effects of the two PE systems in terms of quantities at the polymeric chain level, we first perform the topological analysis on the systems by using the Z1 method [40–43]. This method is used for identification of entanglement and calculation of the entanglement length. By performing Z1 analysis, the movement of single polymer chains, the number of interior 'kinks', Z, and the entanglement length N_e are introduced here. Z is proportional to the number of entanglements per chain, while N_e is defined as the ratio between chain length N and the number of entanglements. For crystalline PE, $Z = 4.052$ and $N_e = 79.136$, while for amorphous PE $Z = 4.806$ and $N_e = 68.870$. When polymers react to the vibration induced

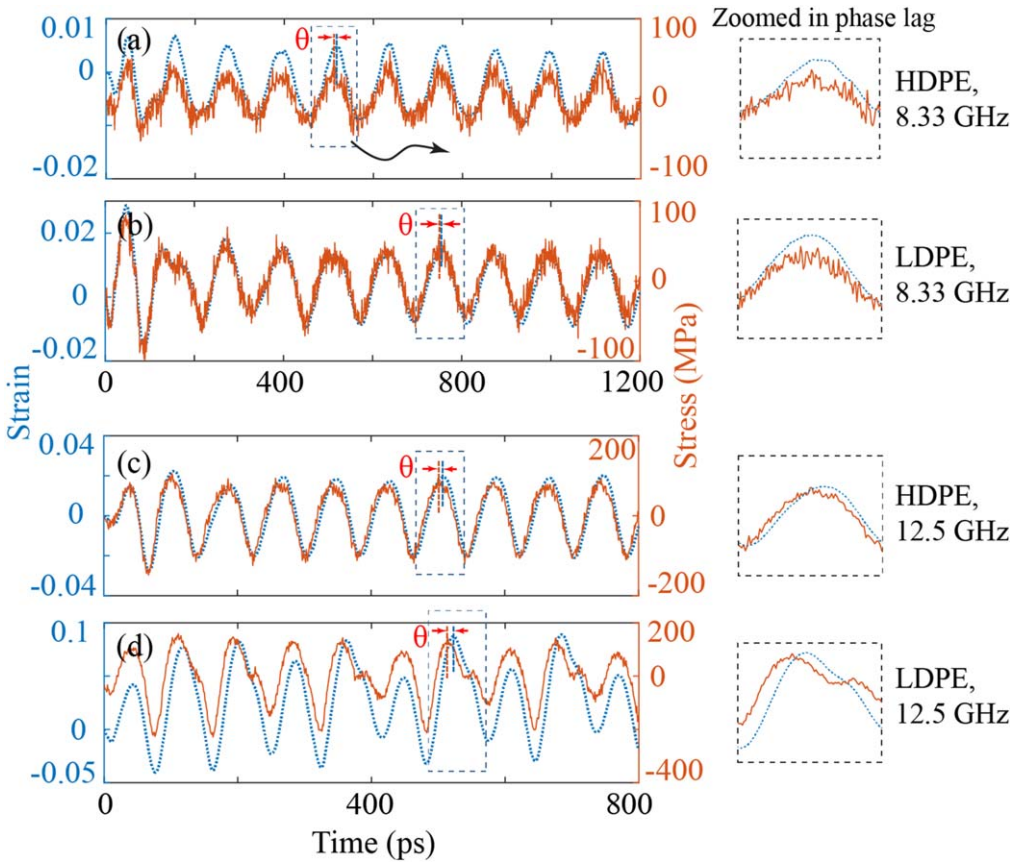

Figure 5. Evolution of stress curves (in red) and strain curves (in blue) and their phase lag θ at a frequency of 8.33 GHz for (a) HDPE and (b) LDPE, plus at a frequency of 12.5 GHz for (c) HDPE and (d) LDPE. Zoom-in graphs to show the phase lag between stress and strain curves are inserted.

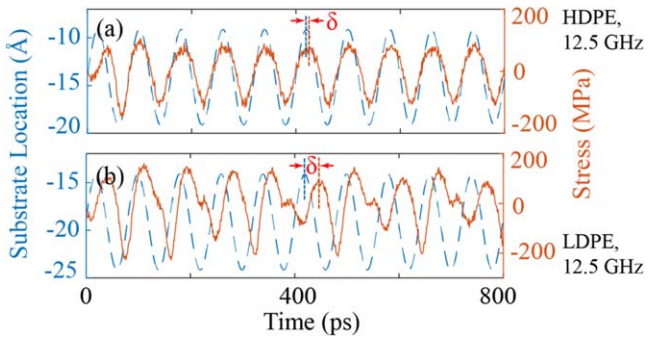

Figure 6. Evolution of substrate movement (in blue) and stress (in red) for (a) LDPE and (b) HDPE at the frequency of 12.5 GHz.

by ultrasonic waves, the entanglements will continuously be created and lost due to the contour length fluctuation (CLF) of the primitive chains. Regarding the reptation mechanism in the tube model [44], the movements of polymeric chains will also lead to a constraint release (CF) when polymeric chains are crawling out of the tube. When CLF and CF happen, the more entangled chains in amorphous PE tend to generate more heat than the less entangled chains in crystalline PE.

The evolution of averaged chain end-to-end distance, $\langle R_{ee} \rangle$, and radius of gyration, $\langle R_g \rangle$, for all polymeric chains in both amorphous PE and crystalline PE systems during actuation are reported in figure 7. From figures 7(a) and (b), it is found the values of end-to-end distance of amorphous PE increases while that of crystalline PE decreases. It shows that the random polymeric coils in amorphous PE tend to extend while the more aligned chains in crystalline PE are crimped slightly. The evolution of radius of gyration in figures 7(c) and (d) provides evidence to this micropicture of polymeric chains when it is excited by the ultrasonic wave. Grouping figures 7(a)–(d), the movements and geometric changes of polymeric chains are more significant at a higher frequency (12.5 GHz) that at a lower frequency. Comparing between the amorphous PE and crystalline PE at the same frequency, the conformational fluctuation of polymeric chains in amorphous PE is more pronounced than crystalline PE, which is the reason for the different ultrasound-induced thermal effects at chain level.

3.2.3. The fluctuation of single atoms. Focusing on the vibration of single atoms, we believe that the discrepancy in the ultrasound-induced motion of atoms in HDPE and LDPE causes the observed difference in their temperature change, because the temperature is a measurement of the average kinetic energy of the system. To examine this hypothesis, we introduce the root mean square fluctuation (RMSF) [45–47], of every PE monomer in the system to evaluate the vibration-induced local mobility of HDPE and LDPE. The expression

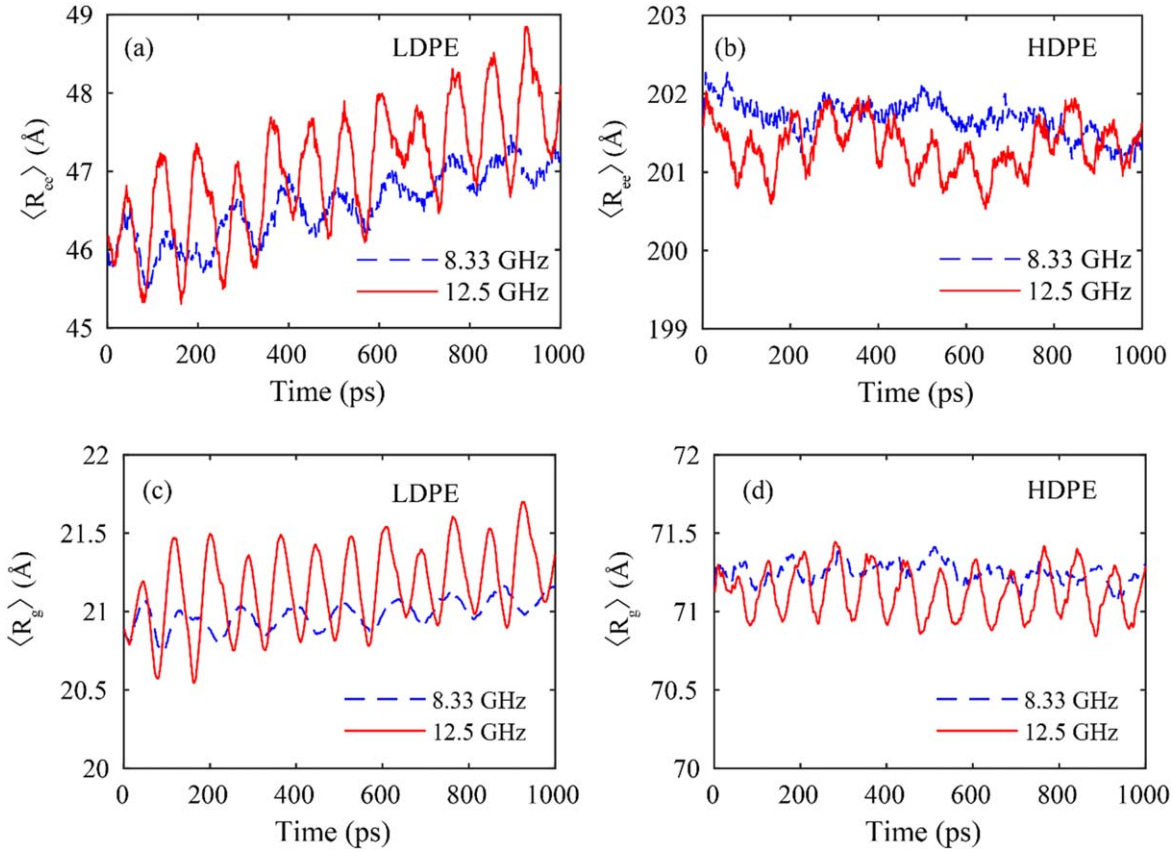

Figure 7. Evolution of average end-to-end distance of polymeric chains for (a) LDPE and (b) HDPE, and average radius of gyration for (c) LDPE and (d) HDPE at the frequencies of 8.33 and 12.5 GHz during the ultrasound-induced heating process.

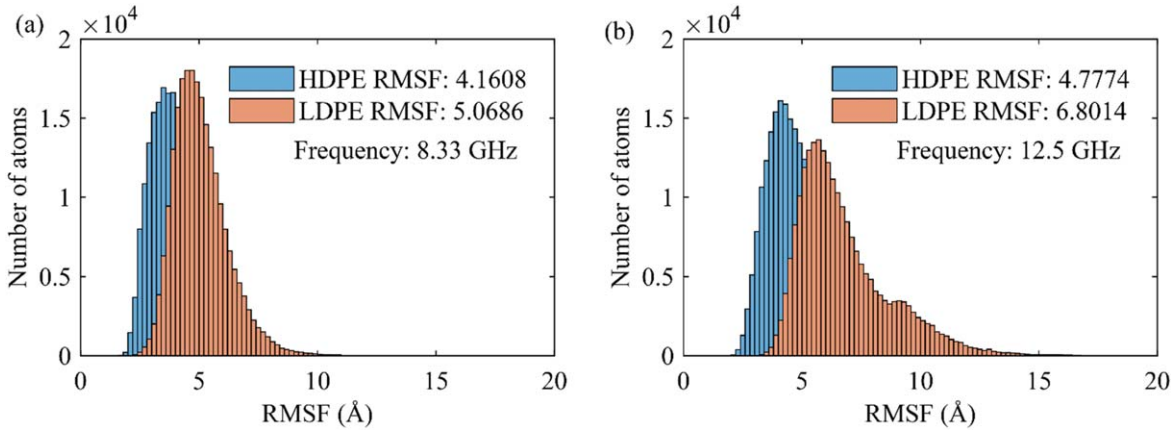

Figure 8. RMSF values of HDPE and LDPE at the frequencies of (a) 8.33 GHz and (b) 12.5 GHz.

of RMSF takes the following format:

$$\mathrm{RMSF}_i = \sqrt{\frac{1}{\tau}\sum_{t=1}^{\tau}(r_i(t) - r_{i,\mathrm{mean}})^2}\,. \qquad (2)$$

Figure 8 shows that the overall RMSF value is lower when the polymer is excited by a lower frequency external vibration. Compared HDPE with LDPE, the flexibility of HDPE with the crystalline structure is much less than that of the amorphous LDPE. The chain movement inside HDPE is less active, which may cause less friction with surrounding chains. It means less heat will be generated due to internal friction. Thus HDPE is less heated by focused ultrasound compared to LDPE.

4. Conclusions

In this work, the HIFU-induced thermal effect on PE was systematically studied by experiments and MD simulations. From

the experiments, we found the heating rate of amorphous LDPE is remarkably larger than the crystalline HDPE under focused ultrasound with the same acoustic power. To investigate the mechanisms behind this phenomenon, MD simulations were performed. In a top-down manner, the mechanisms were investigated at different conformational scales. At the entire system level, we found the frequency-dependent viscoelasticity is the direct factor. It was shown the amplitude of cyclic stress σ_0, strain ϵ_0, and the corresponding phase lag θ, determine the ultrasound-induced thermal effect on PE. When the polymers react to ultrasonic waves, LDPE has a larger phase lag θ than HDPE, and results in a larger heating rate. With the increase of frequency, the increases of σ_0 and ϵ_0 are the proximate causes of fast heating in response to the HIFU. Second, at the molecular chain level, we found the thermal motion of chains in LDPE is larger than HDPE by analyzing the conformational quantities, the end-to-end distance and radius of gyration. Last, the parameter RMSF indicates the atoms inside LDPE are more flexible than HDPE on average. In conclusion, this study can establish a rigorous link between molecular constitute and macroscopic mechanical properties, i.e. between polymer chemistry and viscoelasticity, for optimal processing, design, and application of polymers in the HIFU fields.

Acknowledgments

Financial support from the NSF CMMI grant 2016474 is gratefully acknowledged.

ORCID iDs

Shima Shahab https://orcid.org/0000-0003-1970-5345
Reza Mirzaeifar https://orcid.org/0000-0003-3427-0714

References

[1] Siegel R A 2014 Stimuli sensitive polymers and self regulated drug delivery systems: a very partial review *J. Control. Release* **190** 337–51
[2] Alvarez-Lorenzo C *et al* 2020 Stimuli-sensitive crosslinked hydrogels as drug delivery systems: impact of the drug on the responsiveness *Int. J. Pharm.* **579** 119157
[3] Bhargava A *et al* 2017 Focused ultrasound actuation of shape memory polymers; acoustic-thermoelastic modeling and testing *RSC Adv.* **7** 45452–69
[4] Bhargava A, Kaiyuan P, Mirzaeifar R and Shahab S 2018 Ultrasound actuated shape-memory polymer based drug delivery containers *Proc. SPIE* **10595** 105852H
[5] Cichosz S, Masek A and Zaborski M 2018 Polymer-based sensors: a review *Polym. Test.* **67** 342–8
[6] Sigolaeva L V *et al* 2018 Surface functionalization by stimuli-sensitive microgels for effective enzyme uptake and rational design of biosensor setups *Polymers* **10** 791
[7] Pasparakis G and Vamvakaki M 2011 Multiresponsive polymers: nano-sized assemblies, stimuli-sensitive gels and smart surfaces *Polym. Chem.* **2** 1234–48
[8] Ze Q *et al* 2020 Magnetic shape memory polymers with integrated multifunctional shape manipulation *Adv. Mater.* **32** 1906657
[9] Appiah C *et al* 2019 Living materials Herald a new era in soft robotics *Adv. Mater.* **31** 1807747
[10] Ware T *et al* 2012 Three-dimensional flexible electronics enabled by shape memory polymer substrates for responsive neural interfaces. *Macromol. Mater. Eng.* **297** 1193–202
[11] Cui H *et al* 2019 Bioinspired actuators based on stimuli-responsive polymers. *Chem.—Asian J.* **14** 2369–87
[12] Mather P T, Luo X and Rousseau I A 2009 Shape memory polymer research *Annu. Rev. Mater. Res.* **39** 445–71
[13] Yakacki C M *et al* 2007 Unconstrained recovery characterization of shape-memory polymer networks for cardiovascular applications *Biomaterials* **28** 2255–63
[14] Lendlein A and Langer R 2002 Biodegradable, elastic shape-memory polymers for potential biomedical applications *Science* **296** 1673–6
[15] Amamoto Y *et al* 2012 Self-healing of covalently cross-linked polymers by reshuffling thiuram disulfide moieties in air under visible light. *Adv. Mater.* **24** 3975–80
[16] Ghosh B and Urban M W 2009 Self-repairing oxetane-substituted chitosan polyurethane networks *Science* **323** 1458–60
[17] Fang L *et al* 2016 solar light responsive polymer composites with three Shape-Memory effects. *Macromol. Mater. Eng.* **301** 267–73
[18] Meng H and Li G 2013 A review of stimuli-responsive shape memory polymer composites *Polymer* **54** 2199–221
[19] Hribar K C, Metter R B and Burdick J A 2009 Novel nano-composite biomaterials that respond to light *2009 Annual International Conference of the IEEE Engineering in Medicine and Biology Society* 2409-11
[20] Bai Y, Zhang J and Chen X 2018 A thermal-, water-, and near-infrared light-induced shape memory composite based on polyvinyl alcohol and polyaniline fibers *ACS Appl. Mater. Interfaces* **10** 14017–25
[21] Ze Q *et al* 2019 magnetic shape memory polymers with integrated multifunctional shape manipulation *Adv. Mater.* **32** 1906657
[22] Small W IV *et al* 2005 Laser-activated shape memory polymer intravascular thrombectomy device *Opt. Express* **13** 8204–13
[23] Maitland D J *et al* 2002 Photothermal properties of shape memory polymer micro-actuators for treating stroke *Lasers Surg. Med.* **30** 1–11
[24] Li J *et al* 2017 Micro/nanorobots for biomedicine: delivery, surgery, sensing, and detoxification *Sci. Robot.* **2** 1-9
[25] Schmidt A M 2006 Electromagnetic activation of shape memory polymer networks containing magnetic nanoparticles *Macromol. Rapid Commun.* **27** 1168–72
[26] Jacobs M A 2005 *Measurement and modeling of thermodynamic properties for the processing of polymers in supercritical fluids* Eindhoven University of Technology
[27] Liu B *et al* 2013 High-Intensity focused Ultrasound-induced thermal effect for solid polymer materials. *Macromol. Chem. Phys.* **214** 2519–27
[28] Bruinewoud H 2005 *Ultrasound-induced drug release from polymer matrices: the glass transition temperature as a thermo-responsive switch* Technische Universiteit Eindhoven.
[29] Lin C K S *et al* 2017 Investigations on the correlation between particle velocity distribution and PMMA heating effect induced by high-intensity focused ultrasound *2017 IEEE International Ultrasonics Symposium (IUS)* 1–4
[30] Ma H and Tian Z 2015 Effects of polymer chain confinement on thermal conductivity of ultrathin amorphous polystyrene films *Appl. Phys. Lett.* **107** 073111

[31] Ma H and Tian Z 2017 Effects of polymer topology and morphology on thermal transport: a molecular dynamics study of bottlebrush polymers *Appl. Phys. Lett.* **110** 091903
[32] Pillai R, Borg M K and Reese J M 2018 Acoustothermal atomization of water nanofilms *Phys. Rev. Lett.* **121** 104502
[33] Li C, Ma H and Tian Z 2017 Thermoelectric properties of crystalline and amorphous polypyrrole: a computational study *Appl. Therm. Eng.* **111** 1441–7
[34] Pillai R, Borg M K and Reese J M 2018 Dynamics of nanodroplets on vibrating surfaces *Langmuir* **34** 11898–904
[35] Peng K, Nain A and Mirzaeifar R 2019 Tracking the origins of size dependency in the mechanical properties of polymeric nanofibers at the atomistic scale *Polymer* **175** 118–28
[36] Peng K and Mirzaeifar R 2020 Interplay of chain orientation and bond length in size dependency of mechanical properties in polystyrene nanofibers *ACS Appl. Polym. Mater.* **2** 1664–71
[37] Plimpton S 1995 Fast parallel algorithms for short-range molecular dynamics *J. Comp. Phys.* **117** 1–19
[38] Yamamoto T 2004 Molecular dynamics modeling of polymer crystallization from the melt *Polymer* **45** 1357–64
[39] Yamamoto T 2008 Molecular dynamics simulations of steady-state crystal growth and homogeneous nucleation in polyethylene-like polymer *J. Chem. Phys.* **129** 184903
[40] Karayiannis N C and Kröger M 2009 Combined molecular algorithms for the generation, equilibration and topological analysis of entangled polymers: methodology and performance *Int. J. Mol. Sci.* **10** 5054–89
[41] Shanbhag S and Kröger M 2007 Primitive path networks generated by annealing and geometrical methods: insights into differences *Macromolecules* **40** 2897–903
[42] Kröger M 2005 Shortest multiple disconnected path for the analysis of entanglements in two-and three-dimensional polymeric systems *Comput. Phys. Commun.* **168** 209–32
[43] Hoy R S, Foteinopoulou K and Kröger M 2009 Topological analysis of polymeric melts: chain-length effects and fast-converging estimators for entanglement length *Phys. Rev.* E **80** 031803
[44] Stephanou P S *et al* 2010 Quantifying chain reptation in entangled polymer melts: topological and dynamical mapping of atomistic simulation results onto the tube model *J. Chem. Phys.* **132** 124904
[45] Chiessi E, Lonardi A and Paradossi G 2010 Toward modeling thermoresponsive polymer networks: a molecular dynamics simulation study of N-isopropyl acrylamide co-oligomers *J. Phys. Chem.* B **114** 8301–12
[46] Bozorgmehr M R *et al* 2014 All atom molecular dynamics simulation study of polyethylene polymer in supercritical water, supercritical ethanol and supercritical methanol *J. Supercritical Fluids* **86** 124–8
[47] Chiessi E, Cavalieri F and Paradossi G 2007 Water and polymer dynamics in chemically cross-linked hydrogels of poly (vinyl alcohol): a molecular dynamics simulation study *J. Phys. Chem.* B **111** 2820–7